Ligand Binding and Subtype Selectivity of the Human A2A Adenosine Receptor: Identification and Characterization of Essential Amino Acid Residues

Jaakola, V.P.; Lane, J.R.; Lin, J.Y.; Katritch, V.; IJzerman, A.P.; Stevens, R.C.

THE JOURNAL OF BIOLOGICAL CHEMISTRY VOL. 285, NO. 17, pp. 13032–13044, April 23, 2010

Ligand Binding and Subtype Selectivity of the Human A_{2A} Adenosine Receptor

*IDENTIFICATION AND CHARACTERIZATION OF ESSENTIAL AMINO ACID RESIDUES**

Received for publication, December 18, 2009, and in revised form, February 8, 2010 Published, JBC Papers in Press, February 10, 2010, DOI 10.1074/jbc.M109.096974

Veli-Pekka Jaakola[‡§1,2], J. Robert Lane[¶1], Judy Y. Lin[¶], Vsevolod Katritch[‡3], Adriaan P. IJzerman[¶], and Raymond C. Stevens[‡‖4]

From the Departments of [‡]Molecular Biology and [‖]Chemistry, The Scripps Research Institute, La Jolla, California 92037, the [§]Oulu Biocenter and Department of Biochemistry, University of Oulu, Post Office Box 3000, 90014 University of Oulu, Finland, and the [¶]Division of Medicinal Chemistry, Leiden/Amsterdam Center for Drug Research, Post Office Box 9502, 2300RA Leiden, The Netherlands

The crystal structure of the human A_{2A} adenosine receptor bound to the A_{2A} receptor-specific antagonist, ZM241385, was recently determined at 2.6-Å resolution. Surprisingly, the antagonist binds in an extended conformation, perpendicular to the plane of the membrane, and indicates a number of interactions unidentified before in ZM241385 recognition. To further understand the selectivity of ZM241385 for the human A_{2A} adenosine receptor, we examined the effect of mutating amino acid residues within the binding cavity likely to have key interactions and that have not been previously examined. Mutation of Phe-168 to Ala abolishes both agonist and antagonist binding as well as receptor activity, whereas mutation of this residue to Trp or Tyr had only moderate effects. The Met-177 → Ala mutation impeded antagonist but not agonist binding. Finally, the Leu-249 → Ala mutant showed neither agonist nor antagonist binding affinity. From our results and previously published mutagenesis data, we conclude that conserved residues Phe-168(5.29), Glu-169(5.30), Asn-253(6.55), and Leu-249(6.51) play a central role in coordinating the bicyclic core present in both agonists and antagonists. By combining the analysis of the mutagenesis data with a comparison of the sequences of different adenosine receptor subtypes from different species, we predict that the interactions that determine subtype selectivity reside in the more divergent "upper" region of the binding cavity while the "lower" part of the binding cavity is conserved across adenosine receptor subtypes.

Extracellular adenosine has an important physiological role both as a signal of metabolic stress and as a modulator of neurotransmitter release (1, 2). Consequently, adenosine receptors (ARs),[5] members of the G protein-coupled receptor (GPCR) superfamily of receptors, play a pivotal role in many tissues throughout the body. Four subtypes of ARs have been identified in humans, A_1AR, A_{2A}AR, A_{2B}AR, and A_3AR, and each AR subtype possesses distinct pharmacological properties, tissue/cellular distribution, and secondary effector coupling (2).

We recently solved the structure of the membrane-spanning heptahelical domain of human A_{2A}AR as a fusion protein with cysteine-free phage T4 lysozyme to 2.6-Å resolution using x-ray crystallography (3). The structure represents one of the inactive states of the receptor with the subtype selective high affinity antagonist ZM241385 (Fig. 1) bound to it, at a relatively low pH of 5.8. ZM241385 is a selective A_{2A}AR antagonist that has intermediate affinity for the human A_{2B}AR, a 500- to 1000-fold selectivity over A_1AR, and little affinity for A_3AR. The A_{2A}AR:ZM241385 crystal structure reveals near atomic resolution details for receptor antagonist interactions, useful in drug discovery applications. Thus, the A_{A2}AR structure-based virtual ligand screening in a recent study demonstrated a >40% hit rate in identification of novel and diverse lead-like chemotypes for adenosine receptor antagonists (4). Many residues shown to be important for ligand binding in previously published mutagenesis studies were also shown to have direct contacts with the bound ligand in the crystal structure. For example, mutations that have been reported to disrupt antagonist and/or agonist interactions, Glu-169(5.30), His-250(6.52), Asn-253(6.55), and Ile-274(7.39), have important ligand binding interactions in the crystal structure (the numbers in parentheses indicate residue number based on the Ballesteros-Weinstein nomenclature (5)). Surprisingly, we found that the binding mode of ZM241385 to its receptor is very different from the binding of ligand to other GPCRs with known crystal structures, the beta-blockers timolol, carazolol, and cyanopindolol co-crystallized with turkey β_1-adrenoreceptor or human β_2-adrenoceptors and retinal co-crystallized with bovine and squid rhodopsin, and binding of these ligands to their cognate receptors has very little overlap with ZM241385 binding to A_{2A}AR when all available receptor structures are superimposed (6). In addition, the orientation of ZM241385 in the binding pocket deviates greatly from that of homology models, which used the rhodopsin structure as a template (7–8). Therefore, models for ligand-A_{2A}AR interac-

* This work was supported in part by Protein Structure Initiative Grant U54 GM074961 (ATCG3D; to R. C. S.) and by the Dutch Top Institute Pharma, Project D1-105 (to J. R. L., J. Y. L., and A. P. IJ.).

[1] Both authors contributed equally to this work.

[2] Supported by the Oulu Biocenter (Finland, 2009), the Sigrid Jusélius Foundation (Finland, 2009), the Orion-Farmos Research Foundation (Finland, 2009), and an FP7 Marie Curie European Reintegration Grant (2009).

[3] Present address: Skaggs School of Pharmacy and Pharmaceutical Sciences, 9500 Gilman Dr., MC 0657, La Jolla, CA 92093-0657.

[4] To whom correspondence should be addressed: The Scripps Research Institute, 10550 North Torrey Pines Rd., GAC-1200, La Jolla, CA 92037. Tel.: 858-784-9416; Fax: 858-784-9483; E-mail: stevens@scripps.edu.

[5] The abbreviations used are: AR, adenosine receptor; GPCR, G protein-coupled receptor; Sf9, *Spodoptera frugiperda*; TBS, Tris-buffered saline; BSA, bovine serum albumin; TM, transmembrane; Gpp(NH)p, guanosine 5′-(β,γ-imido)triphosphate; ELISA, enzyme-linked immunosorbent assay; NECA, 5′-*N*-ethylcarboxyamidoadenosine.

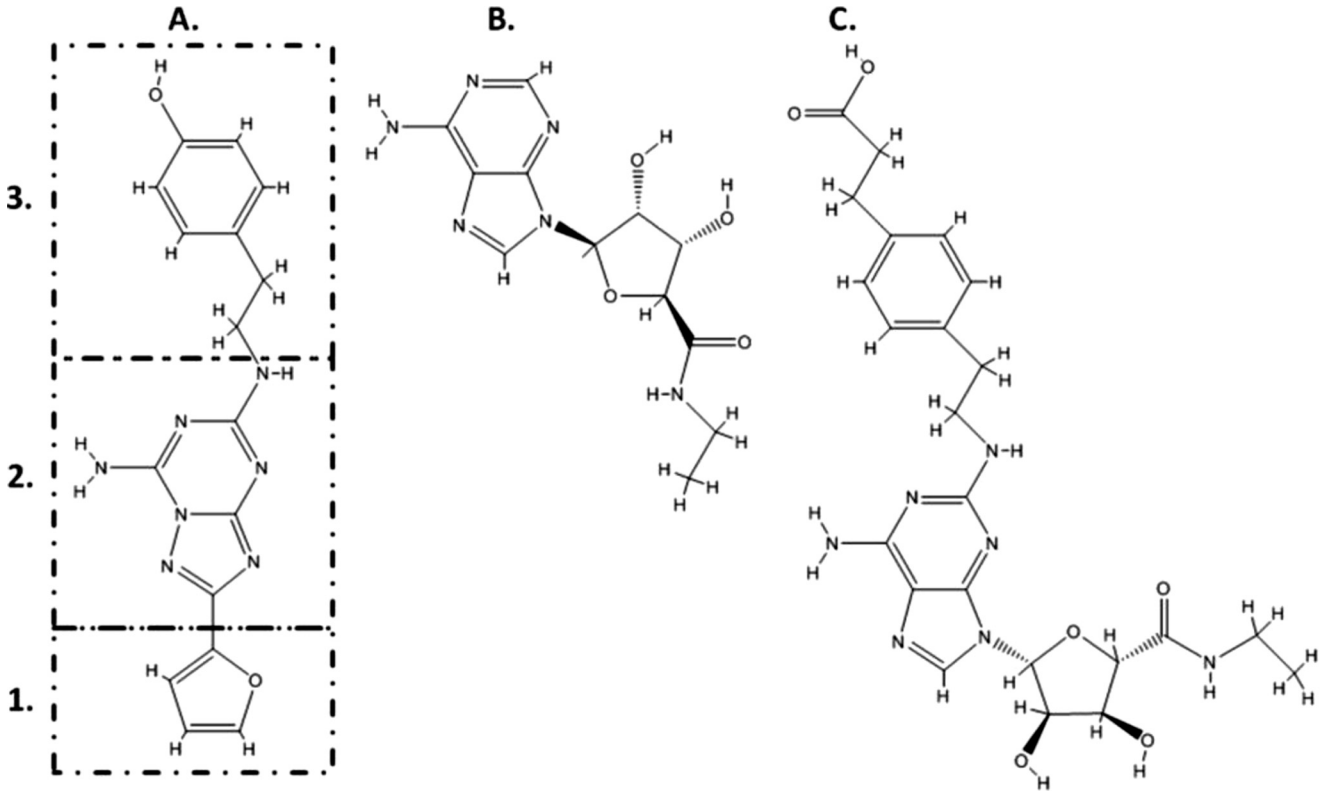

FIGURE 1. **Set of prototypical antagonist and agonists for human A_{2A}AR used in this study.** *A*, ZM241385, a subtype-selective antagonist for human A_{2A}AR (K_i of 260 nM for human A_1AR, 0.8 nM for A_{2A}AR, 32 nM for A_{2B}AR, and >10,000 nM for A_3AR, respectively). *B*, NECA, a relatively non-selective agonist for human ARs (K_i of 14 nM for human A_1AR, 20 nM for A_{2A}AR, 330 nM for A_{2B}AR, and 67 nM for A_3AR, respectively). *C*, CGS21680, a relatively selective agonist for human A_{2A}AR (K_i of 290 nM for human A_1AR, 27 nM for A_{2A}AR, 361,000 nM for A_{2B}AR, and 67 nM for A_3AR, respectively). *Dotted boxes* in *A* are as follows: *1*, furan ring extension of ZM241385; *2*, bicyclic triazolotriazine core of ZM241385 with exocyclic amino group; and *3*, phenoxyethylamino substituent of ZM241385.

tions based upon these other GPCR-ligand structures can give only rough picture of ligand binding (9).

To better understand which of the interactions between ZM241385 and A_{2A}AR found in the crystal structure are biologically significant, to identify which interactions are specific to ZM241385 binding and which interactions are also used for binding other A_{2A}AR ligands, and to predict which regions of the binding pocket contribute to ligand specificity between AR subtypes, we have combined site-directed mutagenesis studies, computer-based molecular docking studies, and sequence analysis of the residues that form the "lower" part of the binding cavity, including interactions with the triazolotriazine core and the furan ring of ZM241385. In particular, we focus on residues shown to be important for ligand binding in the crystal structure but for which no mutagenesis data has been previously reported, namely: Phe-168(5.29), Met-177(5.38), and Leu-249(6.51). In addition, we have extended these studies to better understand the binding of agonists as well as the antagonist ZM241385. We characterize both the wild-type receptor and the mutated receptors for their functional activity (effects on cAMP production) and their ability to bind not only the subtype-selective antagonist ZM241385 but also CGS21680, a subtype selective A_{2A}AR agonist, and NECA, a non-selective AR agonist. Through these studies we confirmed the critical role of Phe-168(5.29), in the aromatic stacking interaction of the (different) bicyclic cores of typical antagonists and agonists. In addition, we demonstrate that Met-177(5.38), which interacts with the furan ring of ZM241385 in the crystal structure, has a less prominent role in the binding of agonists that lack this furan group and that mutation of Leu-249(6.51) to Ala has a surprisingly strong unfavorable effect on both prototypical antagonist and agonist binding to the A_{2A}AR. Adding considerations from sequence analysis and molecular modeling to our observations, we conclude that the binding surface and interaction of the "lower" part of ZM241385 and similar antagonists is conserved between different AR subtypes and species, suggesting that the interactions that determine subtype selectivity reside in the more divergent "upper" region of the binding cavity.

EXPERIMENTAL PROCEDURES

Site-directed Mutagenesis—The plasmid pBac5b+830400+A_{2A}AR containing human A_{2A}AR (3) served as wild-type control and as template for site-directed mutagenesis. Mutagenic primers were designed to change codons for Phe-168 → Ala (gctgcggggagggccaagtggcctgtctcgctgaggatgtggtccccatgaactacatgg)/Trp (gctgcggggagggccaagtggcctgtctctgggaggatgtggtccccatgaactacatgg)/Tyr (gctgcggggagggccaagtggcctgtctctatgaggatgtggtccccatgaactacatgg), Met-177 → Ala (tctttgaggatgtggtccccatgaactacgcggtgtacttcaacttctttgcctgtgtgc), and Leu-249 → Ala (tggggctctttgccctctgctggctgcccgcacacatcatcaactgcttcactttcttct) amino acids (mutations are indicated by underlines). Mutations were made using site-directed mutagenesis utilizing standard PCR techniques beginning with an initial denaturing temperature of 95 °C for 30 s, then 18 cycles of 95 °C for 30 s, 55 °C for 1 min, and 68 °C for 7 min. Subcloning into pcDNA3.1(−) was performed using PCR with primer pairs encoding endogenous

restriction sites BamHI at the 5′ (GGA TCC ATG AAG ACG ATC ATC GCC CTG AGC TAC ATC TTC TG) and HindIII at the 3′ (AAG CTT CTA ATG GTG ATG GTG ATG GTG ATG GTG ATG GTG AGG) termini of pBac5b+830400+A_{2A}AR with subsequent ligation into the corresponding restriction sites found in pcDNA3.1(−). All DNA sequences and mutations were verified by automated API sequencing.

Sf9 Baculoviral Overexpression—Recombinant baculovirus (>10^8 viral particles per ml) was prepared according to a standard transfection protocol from Expression Systems (available on-line). Briefly, high titer recombinant baculoviruses were generated by co-transfecting 2 μg of transfer plasmid containing the target coding sequence with 0.5 μg of Sapphire™ baculovirus DNA (Orbigen) into *Spodoptera frugiperda* (Sf9) cells using 6 μl of FuGENE 6 transfection reagent (Roche Applied Science) and Transfection Medium (Expression Systems). Cell suspension was incubated for 3–4 days while shaking at 27 °C. P-0 viral stock was isolated after 4 days and used to produce high titer baculovirus stock. Expression of gp64 was detected by staining with gp64-PE. Viral titers were determined by a flow cytometric method (10).

Transfection of HEK293T Cells—HEK293T cells were grown as monolayers in Dulbecco's modified Eagle's medium supplemented with 2 mM glutamine and 10% newborn calf serum at 37 °C in a moist, 7% CO_2 atmosphere. Cells were transfected with the indicated plasmids using *N*-[1-(2,3-dioleooxy)propyl]-*N*,*N*,*N*-trimethylammonium methyl sulfate (made in-house, University of Leiden). Experiments were performed 48 h after transfection.

Flow Cytometric Analysis of Cell Surface Expression and Total Protein Expression—To detect plasma membrane-bound and cytosolic receptors, a flow cytometric expression assay was performed as previously described (10). Briefly, commercial monoclonal M2-anti-FLAG antibody (5 μg, Sigma-Aldrich) or monoclonal antibody 856 anti-APJ (7 μg, R&D Systems, Minneapolis, MN) were conjugated with 26 μl of Alexa-488-chromophore (Invitrogen, Eugene, OR) according to the manufacturer's protocol. Alexa-488 conjugated monoclonal antibody 856 was diluted 7-fold in Tris-buffered saline (TBS: 20 mM Tris, pH 7.5, 150 mM NaCl) containing 4% bovine serum albumin (BSA), while the Alexa-488 conjugated FLAG antibody was diluted 10-fold with TBS containing 4% BSA and 0.1% Triton X-100. To measure expression, 10 μl of cell culture was mixed with 15 μl of the Alexa-488-antibody-diluted conjugation solution. The reaction was incubated at 4 °C for 20 min and then diluted 5-fold with TBS to a final volume of 200 μl. The reactions were assayed for fluorescence using a Guava Easycyte microcapillary flow cytometer (Hayward, CA), utilizing laser excitation of 488 nm and emission of 532 nm.

Raw Membrane Isolation for Binding Studies and Immunoblotting—The following protocols were all carried out on ice or at 4 °C unless otherwise noted.

Sf9 Cells—Frozen aliquots of cells were thawed and then resuspended in homogenization buffer (50 mM Hepes, pH 7.4). The cells were subjected to homogenization using a Nitrogen Cavitation Pump (30 min, 800 p.s.i.) following 30 strokes with a Dounce homogenizer. The cell debris and nucleolus were removed by centrifugation at 900 × *g* for 10 min, followed by centrifugation at 100,000 × *g* for 45 min to isolate the raw membrane fraction. The resulting membrane pellet was resuspended in buffer containing 20 mM Hepes, pH 7.4, 800 mM NaCl, and the protein concentration was assayed using the BCA protein assay kit from Pierce using BSA as a standard for the protein assay.

HEK293T Cells—Cells were detached from the plates by scraping them into 5 ml of phosphate-buffered saline, collected, and centrifuged at 200 × *g* for 5 min. Cell pellets were resuspended in 20 ml of ice-cold 50 mM Tris-HCl buffer, pH 7.4. An Ultra-turrax was used to homogenize the cell suspension. The cytosolic and membrane fractions were separated using a high speed centrifugation step of 100,000 × *g* (31,000 rpm in a Beckman Optima LE-80K ultracentrifuge) at 4 °C for 20 min. The pellet was resuspended in 10 ml of Tris buffer, and the homogenization and centrifugation steps were repeated. The resulting pellet was resuspended in 50 mM Tris-HCl buffer, pH 7.4. Adenosine deaminase was added to a final concentration of 0.8 IU/ml.

Saturation Isotherm and Competition Binding Experiments Using Sf9 Membranes—Prior to the ligand binding assays, the membrane pellets were resuspended in ligand binding buffer with either a low salt concentration (TME: 50 mM Tris-HCl, 10 mM $MgCl_2$, 0.5 mM EDTA, pH 7.4) or a high salt concentration (same TME buffer supplemented with 1000 mM NaCl). The samples were tested for binding with [2-^{3}H]-4-(2-[7-amino-2-{2-furyl}{1,2,4}triazolo{2,3-a}{1,3,5,}triazin-5-yl amino]ethyl)-phenol ([^{3}H]ZM241385, 27.4 Ci/mmol), which was obtained from ARC Inc. (St. Louis, MO). Crude plasma membranes (0.2 μg of total protein per reaction) were incubated for 30 min at room temperature with serial dilutions of the radioligand (0.05–10 nM). Incubations were rapidly terminated by filtration using a Tomtec Mach III cell harvester (Tomtec) through a 96-well GF/B filter plate (MultiScreen Harvest plate, Millipore Corp.), and rinsed five times with 500 μl of ice-cold buffer (50 mM Tris-HCl, pH 7.4). The harvest filter plates were dried, and 30 μl of OptiPhase-HiSafe III scintillation liquid (Perkin-Elmer Life Sciences) was added. The bound radioactivity was measured using a PerkinElmer Wallac Jet 1450 Microbeta Scintillation Counter. Nonspecific binding was determined in parallel reactions in the presence of an excess of theophylline (100 μM, Sigma-Aldrich), and specific binding was defined as the difference between total and nonspecific binding. Protein concentrations were determined with the BCA protein assay (Pierce), using BSA as a reference. All incubations were performed in triplicate, and independent experiments were repeated at least two times. Equilibrium dissociation constants (K_d) and maximal receptor levels (B_{max}) were calculated from the results of saturation experiments using GraphPad Prism version 4 software.

For competition binding studies, the membranes were resuspended in ice-cold binding buffer (TME: 50 mM Tris-HCl, 10 mM $MgCl_2$, 0.5 mM EDTA, pH 7.4), containing protease inhibitors (Complete protease inhibitor mixture tablet, Roche Applied Science) and homogenized for 30 strokes with a Dounce homogenizer. Crude plasma membranes (5–20 μg of total protein per reaction) were incubated for 60 min at room temperature with radioligand [^{3}H]ZM241385 concentration

close to the equilibrium dissociation constant (2 nM) and using 10–14 different concentrations of the competing unlabeled ligands. The GTP dependence of agonist binding was investigated with the stable GTP analog Gpp(NH)p (10 μM). Reactions were rapidly terminated by filtration and counted as described above. All incubations were performed in triplicate, and independent experiments were repeated at least twice.

Competition Binding Assays Using HEK293T Membranes—[^{3}H]ZM241385 (27.4 Ci/mmol) was obtained from ARC Inc. NECA and CGS21680 were obtained from Sigma. All other materials were purchased from commercial sources and were of the highest available purity. Binding assays were performed in a 100-μl reaction volume. The assay mixture contained 50 mM Tris-HCl buffer, pH 7.4, membrane protein (25 μg/assay point for single point assays, 5 μg/assay point for competition curves). The ability of increasing concentrations of the antagonist ZM241385 and agonists NECA and CGS21680 to compete with [^{3}H]ZM241385 for binding to the various A_{2A}AR constructs was tested in the absence or presence of 1000 mM NaCl. Nonspecific binding was determined in the presence of an excess of CGS21680 (100 μM). The radioligand concentrations were close to equilibrium dissociation constants ($K_d \sim 1.0$ nM). Incubation was for 2 h at 25 °C. Binding reactions were terminated by filtration through Whatman GF/B filters under reduced pressure using a MY-24 cell harvester (Brandell). Filters were washed three times with ice-cold buffer and placed in scintillation vials. Radioactivity was determined using a Tri-Carb 2900TR liquid scintillation analyzer (PerkinElmer Life Sciences).

Cell-surface Receptor Measurement and Enzyme-linked Immunosorbent Assay—Transfected cells were seeded in 48-well plates (Costar). After 48 h of incubation, the monolayers were washed once with TBS (50 mM Tris, 150 mM NaCl (pH 7.5)) and fixed for 30 min with 4% paraformaldehyde in phosphate-buffered saline. Subsequently, cells were washed three times with TBS and, where appropriate, permeabilized with 0.5% Nonidet P-40 in TBS. After 30 min, the permeabilization solution was replaced with blocking buffer (1% fat-free milk, 0.1 M $NaHCO_3$ (pH 8.6)), and the cells were incubated for 4 h at room temperature. Then, the blocking buffer was replaced with the primary antibody solution containing a 1:1000 dilution of anti-FLAG (M2) antibody (Sigma) in TBS with 0.1% BSA. The cells were incubated overnight at 4 °C with shaking. The monolayers were washed three times with TBS, after which the secondary antibody containing a 1:2500 dilution of Goat-anti-mouse IgG-horseradish peroxidase conjugate (Bio-Rad) was added. After 2 h of incubation at room temperature, the cells were washed three times with TBS and the OPD substrate solution (5 mM *O*-phenylenediamine (Sigma), 0.03% H_2O_2 in 0.1 M citrate-phosphate buffer (pH 5.0)) was applied for ~10 min. The reaction was stopped by the addition of 1 M H_2SO_4, samples were taken from the supernatants, and the optical density was measured in a Victor2 Wallac multilabel counter at 490 nm.

Demonstration of Downstream Signaling by Intracellular cAMP Determination—HEK293T cells were grown and transfected as described above. Experiments were performed 48 h after transfection. Cells were harvested, resuspended in stimulation buffer and added to 384-well OptiPlates at a concentration of 7500 cells/well. The assay was performed following the protocol recommended in the LANCE cAMP 384 kit (PerkinElmer Life Sciences). The assay tracer, antibody, and detection mix are components of the kit. Deviations from the kit protocol are as follows. The stimulation buffer used was phosphate-buffered saline with the addition of 5 mM HEPES, 0.1% BSA, 50 μM rolipram, 50 μM cilostamide, and 0.8 IU/ml adenosine deaminase. The assay was performed in white 384-well OptiPlates (PerkinElmer Life Sciences). Treatment of cells with agonist or antagonist was for 45 min. Following addition of the detection/antibody mix plates were left for 3 h prior to reading using a VICTOR2 plate reader (PerkinElmer Life Sciences).

SDS-PAGE Immunoblotting—Equal amounts of Sf9 total membranes from the wild-type and mutant samples were separated on identical 12% SDS-polyacrylamide gels (Pre-Cast Gels, Bio-Rad Laboratories) and electroblotted using a semi-dry cell (Bio-Rad Laboratories) to methanol-treated (20 s) and TBS buffer-soaked polyvinylidene difluoride membranes. The blots were incubated overnight with 5% fat free milk, TBS buffer, 0.5% Tween 20. One blot was incubated with monoclonal anti-FLAG M2 antibody (Sigma, 1:5,000) in TBS containing 0.5% Tween 20 and 5% nonfat dry milk for 1 h. A second blot was incubated with monoclonal anti-A_{2A}AR antibody epitope against the receptor's third intracellular loop (Millipore, 1:10,000) in the same buffer. Blots were washed 3 × 20 min with TBS-Tween 20 and then incubated with horseradish peroxidase-conjugated anti-mouse IgG (Amersham Biosciences, 1:50,000) for 1 h. The blots were washed 5 × 20 min and visualized with an ECL-plus chemiluminescence kit (Amersham Biosciences).

Docking and Molecular Modeling—The 3EML crystal structure was used for molecular docking. Two different approaches were used for adding hydrogens atoms: default parameters for protonation in the docking program FlexX or from the program H++ (available on-line from Virginia Tech). The program FlexX was used for docking procedures. Residues within a sphere of 9 Å from ZM241385 were included as belonging to the binding cavity, otherwise default parameters were used. In case of mutations, the corresponding side chains were changed using the program PyMOL and energy-minimized with the Swiss PDBViewer suite.

Model Refinement and Binding Energy Evaluation—Initial docking models of ligand-receptor complexes were refined using ICM conformational modeling (11), and their relative binding energy was evaluated as described previously (12). The energy functions included the following ICM terms with the corresponding default weights: van der Waals ("vw" and "14"), hydrogen bonding ("hb"), distant dependent electrostatics ("el"), torsion ("to"), and desolvation term ("sf," surface tension of 0.004). The global optimization procedure was performed in internal coordinates with free torsion variables in the ligand and the side chains of the binding pocket, as defined by 9-Å distance from the ligand atoms in the PDB entry 3EML.

Data Analysis—The results were analyzed using Prism (Version 4.03 or 5.0, GraphPad, San Diego, CA). The values are mean values ± S.E. of at least two independent experi-

ments performed in triplicate. The concentrations that inhibited half of radiolabeled ligand binding (IC_{50}) and the apparent affinities (apparent K_i) of each ligand for each receptor variant were determined by using nonlinear regression analysis and applying the Cheng-Prusoff equation (13), assuming one-site binding. For agonist binding, both one-site binding and two-site binding models were tested. The EC_{50} is the concentration of agonist that evoked half of the maximal response in functional cAMP assays. For homogeneous competition-based maximum receptor density (B_{max}) and ligand binding affinity (K_d) determination, the following equation was used: $B_{max} = (B_o\ IC_{50})/[L]$, $K_d = IC_{50} - [L]$; where B_o is specifically bound ligand and L is ligand concentration.

Ballesteros-Weinstein Nomenclature—To compare GPCR family A members, we have used the Ballesteros-Weinstein double-numbering system (5). Along with numbering their positions in the primary amino acid sequence, the residues have numbers in parentheses (X.YZ) that indicate their position in each transmembrane (TM) helix (X), relative to a conserved reference residue in that TM helix (YZ). This residue is arbitrarily assigned the number 50. However, the numbering is not used in the extra/intracellular regions beyond residues TM.20 or TM.70, as these are highly divergent loop regions that cannot be reliably aligned.

RESULTS

Selection of Amino Acid Residues of A_{2A}AR for Further Ligand Binding Cavity Analysis—An x-ray crystal structure analysis of the human A_{2A}AR-ZM241385 complex revealed 11 residues that are in direct contact with ZM241385 (Fig. 2). The PDB-deposited structure (3EML) reveals that these form 75 atomic receptor-ligand contacts with a distance of <4 Å. Additionally, ZM241385 makes several atomic contacts with crystallographic water molecules. Fig. 3 shows a multiple

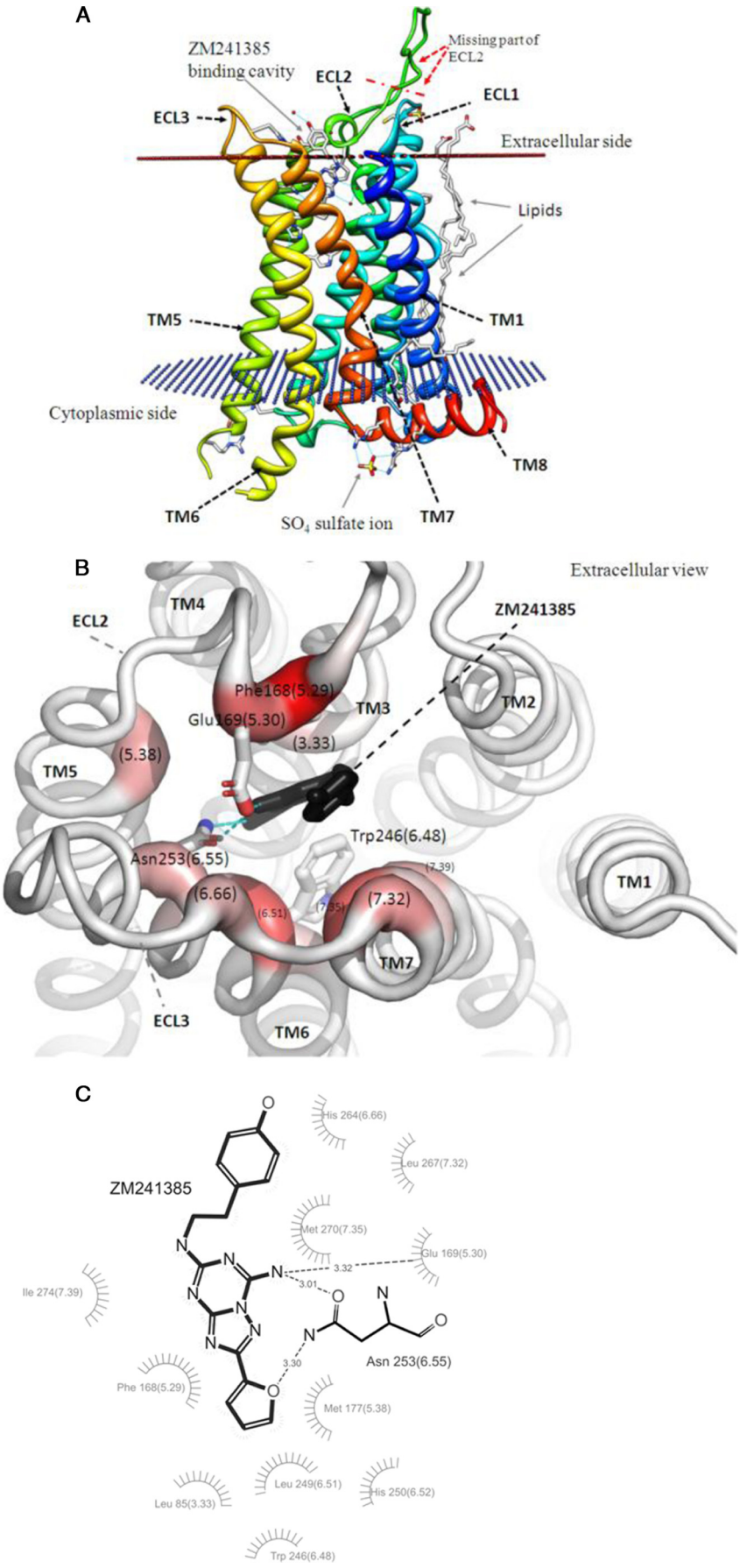

sequence alignment of AR subtypes across a number of species. The TM domains, including the lower part of the ZM241385-binding cavity, are highly conserved among receptors from different species (Fig. 3*A*), and the extracellular domains and upper part of the ZM241385 binding site are somewhat less conserved (Fig. 3, *A* and *B*). We sub-classified the residues shown to interact with ZM241385 in the co-crystal structure into four partially overlapping categories. The first category consists of residues that interact with the furan ring: (Leu-85(3.33), Met-177(5.38), Trp-246(6.48), Leu-249(6.51), His-250(6.52), and Asn-253(6.55)) (Figs. 2*C* and 3*B*). These residues are mainly located in TMs 3, 5, 6, and 7 and hold the furan ring in close proximity to these TMs while stabilizing the so-called "toggle-switch" Trp-246(6.48) side-chain rotamer in the inactive conformation. The second category consists of the residues that make contacts with the bicyclic triazolotriazine core unit of ZM241385: Phe-168(5.29), Glu-169(5.30), Asn-253(6.55), and Ile-274(7.39). The third category consists of the residues that are close to the *4-hydroxyphenyl group* of ZM241385: Leu-267(7.32), His-264(6.66), and Met-270(7.35). Notably, non-xanthine A_{2A}AR ligands with a ZM241385-like bicyclic/tricyclic core unit have a large chemical variability in this third area of the pharmacophore. Furthermore, in the PDB-deposited model, large atomic temperature factors (*B*-factors) are associated with the *4-hydroxyphenyl group* of ZM241385, an indication of local structural flexibility. The fourth category includes those amino acid residues that make interactions with crystallographic waters in the structure. The major contribution to the binding of ZM241385 is derived from residues in classes one, two, and four (Table 1 and Figs. 2*C* and 3*B*). Surprisingly, a literature review reveals that the majority of these residues has neither been recognized as binding residues *in silico* nor studied biochemically such as in mutagenesis experiments (for recent review, see Ref. 14). In the present study we focused on the first and second categories, selecting amino acid residues that are in direct contact with ZM241385 but for which no mutagenesis data is available from the published literature: namely residues Met-177(5.38); Phe-168(5.29), and Leu-249(6.51) (Table 1). We examined these by constructing mutant receptors in which the selected residues were replaced with alanine or in the case of Phe-168(5.29), with alanine, tyrosine, or tryptophan.

Functional Expression of Wild-type and Mutated Receptors—To verify that mutated receptors were well expressed and properly localized to the cell surface, we measured total receptor levels (SDS-PAGE followed by immunoblotting) in comparison to the amount of receptor detected on the surface of non-permeabilized cells (flow cytometry using fluorescently labeled anti-receptor antibodies). Wild-type and mutated receptors were expressed to approximately equal levels in Sf9 baculovirus cells (Table 2). When transiently expressed in HEK293T cells, the relative expression levels of the mutant receptors varied as compared with the wild-type, with Phe-168(5.29) mutants all having greater expression, and Met-177(5.38) → Ala and Leu-249(6.51) → Ala displaying lower expression. All mutant receptors demonstrated significant cell surface expression, with a similar fraction of total receptors at the cell surface (~0.5–0.6). Thus, wild-type and mutated receptors were properly localized on the cell surface in both expression systems (Table 2).

Binding Properties in G Protein-restricted Environment Using Sf9 Membranes—To evaluate the contributions of different residues to ligand binding, we examined the saturation binding isotherms of the wild-type and mutated receptors expressed in Sf9 membranes for a radiolabeled antagonist ([^{3}H]ZM241385). When compared with the wild-type receptor, the Phe-168(5.29) → Tyr and Phe-168(5.29) → Trp mutations showed an 8- and a 4-fold decrease, respectively, in [^{3}H]ZM241385 binding affinity (Table 3). Mutation of this residue to a small apolar residue, Phe-168(5.29) → Ala, eliminated binding to [^{3}H]ZM241385. The Met-177(5.38) → Ala mutation reduced the binding affinity of [^{3}H]ZM241385 by 8-fold and the Leu-249(6.51) → Ala mutant showed no measurable radioligand binding for [^{3}H]ZM241385.

Binding Properties in G Protein-balanced Environment Using HEK293T Membranes—Sf9 cells represent an essentially G protein-free environment. For analysis of agonist binding, it is important to use a more native expression system for G proteins, such as transient expression in HEK293T cells. Expression in HEK293T cells also allows determination of the functional effects of the binding site mutations on receptor-mediated G protein signaling. To directly compare the ligand-binding properties of wild-type and mutated A_{2A}AR expressed in these two different cell lines, we verified that their ligand-binding properties were similar. A single point radioligand binding assay using a saturating concentration of [^{3}H]ZM241385 (20 nM) revealed no specific binding to the Phe-168(5.29) → Ala or Leu-249(6.51) → Ala mutated receptors, in agreement with the data obtained using Sf9 cell membranes. Receptor densities based on homologous competition binding assays of [^{3}H]ZM241385 to either wild-type, Phe-168(5.29) → Tyr, Phe-168(5.29) → Trp, or Met-177(5.38) → Ala mutated receptors were measured to be 3.5 ± 0.4 pmol/mg, 0.8 ± 0.1 pmol/mg, 3.4 ± 0.3 pmol/mg and 1.6 ± 0.2 pmol/mg of protein, respectively (Table 3). The binding affinity of Phe-168(5.29) → Tyr and Met-177(5.38) → Ala mutated receptors for [^{3}H]ZM241385 determined in homologous competition

FIGURE 2. **ZM241385 binding mode and receptor-ZM241385 interactions.** *A*, receptor:ligand:lipid:metal ion backbone representation of the structure of human A_{2A}AR-T4 lysozyme fusion protein with ZM241385 bound (PDB ID: 3EML). The missing part of extracellular loop 2 is modeled onto the structure (beginning and ending points are indicated by the *dotted red line*). The T4 lysozyme fusion protein domain is omitted from the figure. The membrane boundary planes are obtained from the Orientations of Proteins in Membranes database (available on-line from the University of Michigan) and marked as "dummy" atoms (*blue-colored* dummy atoms in the cytoplasmic region and *red-colored* dummy atoms at the extracellular site). The receptor is colored *blue* at the amino terminus and changes gradually to *red* at the carboxyl terminus. Lipid, ligand, and sulfate ions are shown as *stick models*, and their polar interactions are shown as *thin blue lines*. Crystallographic waters in the binding cavity are shown as *red balls*. *B*, extracellular view of the ZM241385-binding cavity. Normalized occluded surface areas were calculated for ZM241385 binding residues and are represented as *thickened red regions* of the backbone chain. Residues are labeled by their corresponding Ballesteros-Weinstein indexing. The polar anchoring residues of Asn-253(6.55), Glu-169(5.30), and toggle-switch residue of Trp-246(6.48) side chains are shown as *stick models*, and polar interactions with ZM241385 (*black*) are indicated as *light blue dotted lines*. *C*, schematic ligand-plot representation of the polar and aromatic interactions between ZM241385 and human A_{2A}AR at the antagonist-binding cavity.

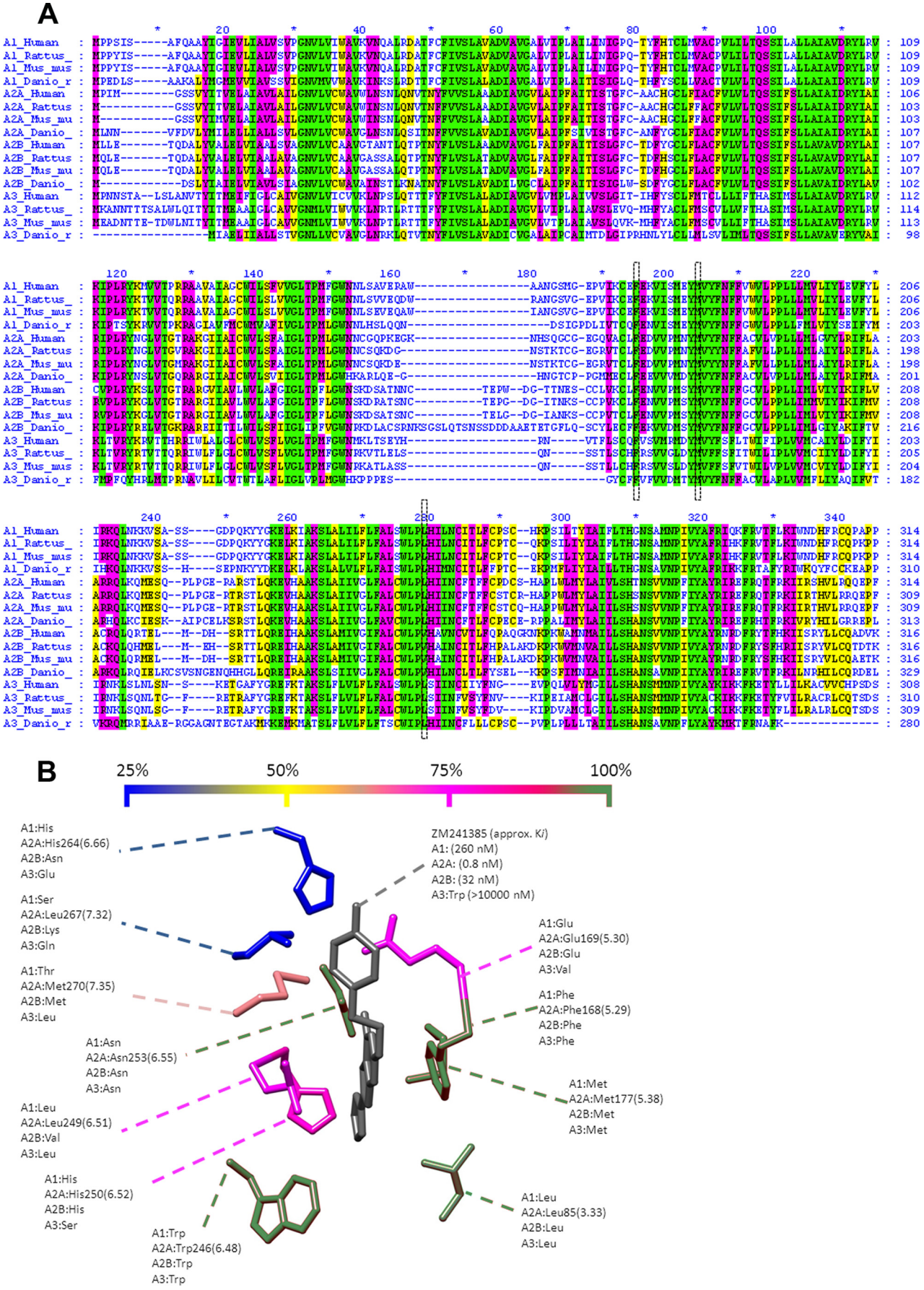

TABLE 1

Calculated contributions of various A_{2A}AR residues to ZM241385 binding; only residues within 4.5 Å of the ligand are shown

Bold font indicates amino acid residues examined in this study. Mutations that are reported to disrupt antagonist and/or agonist binding are indicated in italic. Contacts that are unfavorable in the crystal structure and improved in the conformationally refined model are shown as underlined text. vdW, van der Waals.

Pocket residues	Contact distance	Energy (3EML)		Energy (refined)	
		Total	vdW	Total	vdW
	Å	kcal/mol			
Phe-168(5.29)	3.2	−6.0	−6.0	−6.4	−6.4
Asn-253(6.55)	3.0	−4.7	−2.3	−5.7	−2.4
Leu-249(6.51)	3.5	−3.5	−3.4	−3.1	−3.0
Glu-169(5.30)	3.4	−4.0	−3.0	−2.1	−1.4
Met-177(5.38)	3.0	−1.3	−1.3	−1.7	−1.6
Ile-274(7.39)	3.9	−1.8	−1.8	−1.4	−1.5
Met-270(7.35)	3.1	15.9	15.8	−1.3	−1.3
Leu-85(3.33)	3.7	−1.2	−1.2	−1.1	−1.1
Trp-246(6.48)	3.4	−0.2	−0.2	−1.1	−1.1
Leu-267(7.32)	3.8	−1.4	−1.4	−0.7	−0.7
Asn-181(5.42)	4.4	−0.4	−0.4	−0.5	−0.4
His-264(6.66)	3.3	−0.1	−0.1	0.0	−0.1
His-250(6.52)[a]	3.4	1.9	1.8	0.7	0.6
Totals		−6.8	−3.4	−24.3	−20.4

[a] Interaction is mediated mainly via crystallographic waters.

assays was decreased 2- and 4-fold, respectively, as compared with wild-type, whereas only 1.5-fold change in affinity for [^{3}H]ZM241385 was observed for the Phe-168(5.29) → Trp mutant (Table 3). These results are consistent with the measurements obtained from receptors expressed in Sf9 cells, although the magnitude of the decreased ligand affinity displayed by the mutated receptors is more modest in the HEK293T cells.

We also determined the effects of these binding site mutations on the ability of the agonists NECA or the A_{2A}AR-selective agonist CGS21680 to compete with [^{3}H]ZM241385 (Table 4). Binding (K_i) of Phe-168(5.29) → Tyr to NECA or CGS21680 was decreased by 13- and 25-fold, respectively, compared with binding of these ligands to the wild-type receptor. In contrast, the affinity of Phe-168(5.29) → Trp for NECA was increased by at least 2-fold, whereas the affinity of this mutant for CGS21680 was similar to the wild-type (Table 4). Interestingly, the affinity of the Met-177(5.38) → Ala mutant for NECA was similar to that of the wild-type receptor, whereas the affinity of this mutant for CGS21680 was decreased by 7-fold. As these two agonists have identical chemical scaffolds, 5′-uronamide adenosine, and differ only in the solvent-exposed C2-substituent that is present in the CGS21680 structure and cannot directly interact with Met-177(5.38), this difference in binding affinity is most likely explained by the higher conformational mobility of NECA in the binding pocket (see also "Discussion").

Functional G Protein Response Using cAMP Assay—We measured receptor activity using intact HEK293T cells transiently transfected with wild-type and mutated receptors. Prototypical A_{2A}AR agonist CGS21680 stimulated adenylyl cyclase activity mediated by both wild-type and mutated receptors. When compared with wild-type receptor, the Phe-168(5.29) → Tyr mutant showed a 4-fold decrease in activity, whereas mutation of this residue to a tryptophan showed a near wild-type EC_{50} value (Table 5). The cAMP assay also revealed that, although the Phe-168(5.29) → Ala mutation resulted in no detectable binding of the radiolabeled antagonist [^{3}H]ZM241385 (Table 3), the agonist CGS21680 could still evoke a response, albeit with a 63-fold lower activity than the wild-type receptor (Table 5). Similarly, the cAMP assay revealed that the mutant Leu-249(6.51) → Ala resulted in an 11-fold decrease in CGS21680 agonist potency compared with wild-type (Table 5). Finally, the mutation of Met-177(5.38) → Ala showed a significant 6-fold decrease in agonist potency consistent with the competition binding data obtained in HEK293T cell membranes (Table 4). The presence of endogenously expressed A_{2B}AR in HEK293T cells prevents measurement of the potency of the non-selective AR agonist NECA.

Automated Docking—We docked ZM241385, NECA, and CGS21680 into the crystal structure at a standard protonation state (as calculated by the H++ server as well as in the FlexX program suite, pH 7.0), and two additional protonation states (pH 5.5 and pH 8.0) (Fig. 4). We used FlexX, which models side chains as rigid moieties, in default mode. We included residues within a 9.0-Å sphere around the ZM241385 binding site without any other constraints (*e.g.* for a polar interaction from Glu-169(5.30), Asn-253(6.55), or aromatic interaction from Phe-168(5.29), and all crystallographic waters were removed. Without any constraints, >95% of the docking results (top 10 solutions obtained per ligand per pH) showed a polar interaction between Asn-253(6.55) and the exo-cyclic amino group of the ligand as well as aromatic stacking interactions between Phe-168(5.29) and either the triazolotriazine core (ZM241385) or adenine ring system (NECA, CGS21680) (Fig. 4). Re-docking of ZM241385 showed the largest variation in the position of the 4-hydroxyphenyl group side chain (Fig. 4*A*). Interestingly, in 5% of the docking results for NECA and in 20% for CGS21680, the ligand was rotated 180 degrees so that the polar interactions with the receptor via Asn-253(6.55)/Glu-169(5.30) and aromatic stacking interactions with receptor via Phe-168(5.29) were approximately correct, but the ribose motif was directed toward the extracellular space. In the remaining docking results for both NECA and CGS21680, the ribose motif interactions were similarly oriented and clustered into two orientations irrespective of the studied protonation states (Fig. 4). In the first conformation, the ribose motif makes a polar interaction with backbone of Ala-81(3.29), and in the second conformation it is in close proximity to Ser-277(7.42) and His-278(7.43). Energy minimization of receptor side chains revealed that in this conformation the ribose group makes polar interactions with Ser-277(7.42) and Thr-88(3.36) (Fig. 4*D*). The latter conformation of the ribose ring is likely to be more rele-

FIGURE 3. **Amino acid sequence alignment and degree of conservation in the ZM241385 antagonist-binding cavity.** *A*, amino acid sequences of AR subtypes from different species (rat, mouse, and zebrafish) were aligned with human subtypes. The multiple amino acid sequences were aligned using the TCoffee algorithm (available on-line). Identical residues are *shaded in green*, >75% conserved residues are *shaded purple*, >50% are *shaded in yellow*, and <25% conserved residues are shown in *blue*. The three residues examined in this study are indicated by *dashed boxes*. *B*, proximal ZM241385-binding cavity: ZM241385 and side chains of interacting residues are shown as *stick models*; ZM241385 is *gray*, and the interacting residues are *colored* as in *A*; the *coloring scale* is shown above the figure. The side-chain variation between human subtypes is denoted.

TABLE 2

Expression levels of wild-type and mutated human A_{2A}ARs

Immunoblot, flow-cytometry, or ELISA analysis of wild-type and mutant A_{2A}AR on the cell surface of intact cells or on isolated membranes from Sf9 and HEK293T cells.

Receptor construct	Sf9			HEK293T, ELISA[c]		
	Immunoblotting[a]	Flow cytometry[b] (% of wild-type)				
		Without permeabilization	With permeabilization	Cell surface (without permeabilization)	With permeabilization	Ratio cell surface/ permeabilized cell
		Mean fluorescence units		*% of wild-type with permeabilization*		
Wild type	Single band; ++	827 (100%)	1085 (100%)	59 ± 4	100 ± 5	0.65
Phe-168(5.29) → Tyr	Single band; +++	1325 (160%)	1377 (127%)	185 ± 4	307 ± 8	0.62
Phe-168(5.29) → Trp	Single band; +++	1152 (139%)	1088 (100%)	109 ± 5	180 ± 7	0.64
Phe-168(5.29) → Ala	Single band; +++	1486 (180%)	1251 (115%)	72 ± 8	116 ± 4	0.66
Met-177(5.38) → Ala	Single band; +++	1227 (148%)	1218 (112%)	38 ± 1	65 ± 2	0.66
Leu-249(6.51) → Ala	Single band; +++	1011 (122%)	1023 (94%)	31 ± 4	83 ± 1	0.48
Negative control	No band, −	180 (22%)	201 (19%)	0 ± 1	2 ± 1	

[a] Immunoblotting was done with anti-FLAG antibodies and anti-A_{2A}AR antibodies using isolated crude membranes. The spot intensity of mutated receptors was visually compared to wild-type; +++, strong immunoreactivity indicating high expression in isolated membranes; ++, clearly detectable immunoreactivity; +, detectable immunoreactivity; and −, no immunoreactivity.
[b] Flow cytometry was done using anti-FLAG antibodies as primary antibodies and fluorescently labeled antibodies as secondary probes.
[c] ELISA was done using anti-FLAG antibodies as a probe. Details for immunoblotting, flow cytometry, and ELISA studies are described under "Experimental Procedures".

TABLE 3

[^{3}H]ZM241385 antagonist binding properties of wild-type and mutated human A_{2A}ARs expressed in Sf9 and HEK293T cells

The table shows mean ± S.E.; minimum two independent experiments, each performed in triplicates. Saturation isotherm binding studies were carried out with membrane homogenates prepared from baculovirus-infected Sf9 cells, and homogeneous competition binding experiments were carried out with membrane homogenates prepared from transiently transfected HEK293T cells as described under "Experimental Procedures."

Receptor construct	Saturation binding characteristics using Sf9 cells				Homologous competition binding characteristics using HEK293T cells			
	K_d	$K_{d(\text{mutant})}/K_{d(\text{wild-type})}$	B_{max}	$B_{max(\text{mutant})}/B_{max(\text{wild-type})}$	K_d	$K_{d(\text{mutant})}/K_{d(\text{wild-type})}$	B_{max}	$B_{max(\text{mutant})}/B_{max(\text{wild-type})}$
	nM	*-fold*	*pmol/mg*	*-fold*	*nM*	*-fold*	*pmol/mg*	*-fold*
Wild-type	1.6 ± 0.4	1	38 ± 3	1	2.4 ± 0.8	1	3.5 ± 0.4	1
Phe168(5.29) → Tyr	13 ± 3	8	16 ± 3	0.4	5.5 ± 0.3	2.2	0.8 ± 0.1	0.2
Phe168(5.29) → Trp	6.4 ± 0.7	4	15 ± 1	0.3	3.6 ± 0.3	1.5	3.4 ± 0.3	1
Phe168(5.29) → Ala	n.s.b.d.[a]		n.s.b.d.		n.s.b.d.		n.s.b.d.	
Met177(5.38) → Ala	12 ± 2	8	10 ± 1	0.3	10.4 ± 1.4	4.3	1.6 ± 0.2	0.5
Leu249(6.51) → Ala	n.s.b.d.		n.s.b.d.		n.s.b.d.		n.s.b.d.	

[a] n.s.b.d., no specific binding detected.

TABLE 4

Ligand binding properties of wild-type and mutant human A_{2A}ARs characterized in [^{3}H]ZM241385 binding assays in competition with NECA or CGS21680

Table shows mean ± S.E.; minimum three independent experiments, each performed in triplicates. Ligand binding affinities (pK_i/K_i values) were determined in [^{3}H]ZM241385 (5–10 nM) inhibition binding experiments using membrane homogenate prepared from transiently transfected HEK293T cells as described under "Experimental Procedures." pK_i/K_i values were calculated by the Cheng-Prusoff equation (Prism 5.0, GraphPad). About 20 μg of membrane protein per incubation was used. Data was analyzed using a one-way analysis of variance analysis with a Bonferroni post-hoc test, as in GraphPad Prism 5.

Receptor construct	Competitor					
	NECA			CGS21680		
	pK_i	K_i	$K_{i(\text{mutant})}/K_{i(\text{wild type})}$	pK_i	K_i	$K_{i(\text{mutant})}/K_{i(\text{wild type})}$
		nM	*-fold*		*nM*	*-fold*
Wild type	7.28 ± 0.23	94 ± 61	1	6.49 ± 0.11	357 ± 75	1
Phe-168(5.29) → Tyr	5.83 ± 0.19[a]	1190 ± 478	13	5.13 ± 0.17[b]	8990 ± 3340	25
Phe-168(5.29) → Trp	7.34 ± 0.18	39 ± 13	0.4	6.38 ± 0.11	534 ± 131	1.5
Phe-168(5.29) → Ala	ND[c]			ND		
Met-177(5.38) → Ala	7.19 ± 0.19	66 ± 31	0.7	5.64 ± 0.09[a]	2440 ± 526	7
Leu-249(6.51) → Ala	ND			ND		

[a] Significant differences in K_i values between the wild-type and each mutant receptor; $p > 0.01$.
[b] Significant differences in K_i values between the wild-type and each mutant receptor; $p > 0.001$.
[c] ND, not determined because specific binding of [^{3}H]ZM241385 detected was <10% of wild-type values.

vant for the agonist-bound state of the receptor, because both Ser-277(7.42) and Thr-88(3.36) have been implicated in agonist, but not antagonist binding (15). *In silico* mutations to Phe-168(5.29) → Ala, Leu-249(6.51) → Ala, and Met-177(5.38) → Ala followed by docking, suggest that these mutations do not have a major impact on ligand orientation (Fig. 4*D*).

Effect of Mutations on Ligand Binding—To understand the effects of the receptor mutations on ligand binding and to identify docked ligand models that are consistent with the functional behavior of the mutated receptors, we performed energy-based refinement of the ligand receptor-ligand models using global energy optimization of the ligand and the pocket side chains in the ICM program (Molsoft, LLC). Refinement of the ZM241385-A_{2A}AR crystal structure itself yielded only minor changes in side-chain positions that relieved some steric strain in the Met-270(7.35) and His-250(6.52) contacts with the ligand. Predicted total and Van der Waals-only contributions of each contact residue to the ligand binding energy are shown in Table 1. This analysis suggests that Phe-168(5.29), Asn-253(6.55), and Leu-249(6.51) make major contributions to

TABLE 5

CGS21680-induced agonist stimulation of cAMP production mediated by wild-type and mutant A_{2A}ARs

Agonist CGS21680-induced cAMP production was measured in transiently transfected HEK293T cells as described under "Experimental Procedures." The table shows mean ± S.E.; minimum two independent experiments, each performed in triplicates. Data were analyzed using a one-way analysis of variance analysis with a Bonferroni post-hoc test, as in GraphPad Prism 5.

Construct	pEC_{50} (EC_{50} nM)	Fold Δ (EC_{50} mutant/EC_{50} WT)
Wild-type	7.63 ± 0.13 (27.5)	1
Phe-168(5.29) → Tyr	7.00 ± 0.07 (102)[a]	4
Phe-168(5.29) → Trp	7.49 ± 0.16 (33.0)	1
Phe-168(5.29) → Ala	5.84 ± 0.14 (1730)[b]	63
Met-177(5.38) → Ala	6.86 ± 0.19 (156)[c]	6
Leu-249(6.51) → Ala	6.51 ± 0.05 (314)[b]	11

[a] Significant differences in pEC_{50} between the wild-type and each mutant receptor; $p > 0.05$.
[b] Significant differences in pEC_{50} between the wild-type and each mutant receptor; $p > 0.001$.
[c] Significant differences in pEC_{50} between the wild-type and each mutant receptor; $p > 0.01$.

ligand binding, that Met-177(5.38) and Ile-274(7.39) make moderate hydrophobic contacts with the ligand, and that the other residues in the binding pocket have a much smaller impact on ligand binding. It should be noted that the contribution of His-250(6.52) to ZM241385 binding is mediated mostly through the structured water molecule ("wa5" in PDB entry 3EML, *B*-factor = 46 Å^2), whereas our calculations did not take this effect into account. More detailed analysis of mutational effects for Phe-168(5.29), Leu-249(6.51), and Met-177(5.38) positions was provided by implicit conformational modeling of modified residues with flexible ligand and receptor side chains.

The results of binding energy predictions for mutant complexes with ZM241385, CGS21680, and NECA are shown in Table 6. For the Phe-168(5.29) position, although mutations to non-aromatic residues were predicted to have a dramatic negative effect on binding, Tyr and Trp side chains were easily accommodated within the structure and yielded only modest drops in binding energy, which is in line with experimental results. For the Leu-249(6.51) mutations, changes to small polar amino acid (alanine) resulted in a lost hydrophobic contact for this residue and a significant drop in binding energy for all ligands. Interestingly, this drop was much less pronounced for the Leu-249(6.51) → Val mutation; valine in this position is present in the A_{2B}AR subtype. For the Met-177(5.38) position, the modeling predicts only minor drops in binding energy for an alanine mutation.

DISCUSSION

The recently solved human A_{2A}AR-ZM241385 co-crystal structure revealed that the prototypical non-xanthine antagonist, ZM241385, binds very differently to the receptor than had been predicted by models based on rhodopsin binding to retinal (7, 8). The long axis of ZM241385 lies orthogonal to the membrane plane and has a large number of interactions with residues in TM domains 5–7, and extracellular loops 2 and 3 (3). The structure of the extracellular domain (extracellular loops 1–3) has little secondary structure and is held together by a network of four disulfide bridges, three of which are unique to ARs (Fig. 2*A*). This novel and relatively rigid architecture of the extracellular domain, together with the unexpected orientation of the ZM241385 ligand, shifts the upper parts of the TM helices when compared with the other known GPCR structures. Indeed, the binding of ZM241385 is very different from and almost perpendicular to that of retinal in rhodopsin/opsin or the beta-blockers timolol, carazolol, and cyanopindolol in the β_1- and β_2-adrenoceptors.

In particular, the previously published models based on the rhodopsin structure misplaced and misoriented the ZM241385 molecule (and similar types of non-xanthine and xanthine ligands), in a position resembling that of retinal or the β-adrenoreceptor antagonists. Although newer models based on β_2-adrenoreceptor structure were able to predict some of the key features and receptor contacts for ZM241385 binding, large scale deviations in extracellular regions of the TM helices in the models, as much as ~6 Å from the solved crystal structure of A_{2A}AR, resulted in inaccurate positioning of the ligand and missed important interactions (for details, see a recent publication (9)).

ZM241385 is a prototypical AR antagonist, composed of a core bicyclic triazolotriazine unit (see Fig. 1, *notation 2*), a furan ring, and a 4-hydroxyphenylethyl side chain (Fig. 1). The furan ring system is located deep in the binding cavity. It may act by helping to keep the receptor in a resting state through stabilization of Trp-246(6.48), the toggle-switch rotamer, in an inactive conformation (Figs. 2 and 3). The central aromatic/triazolotriazine core system makes polar interactions with the highly conserved Asn-253(6.55) and Glu-169(5.30) residues and hydrophobic interactions with equally conserved Phe-168(5.29) and Ile-274(7.39) side chains. The *triazolotriazine* core unit of ZM241385 also makes a number of polar interactions with ordered water molecules filling the solvent-exposed part of the open binding cavity (Fig. 2).

The 4-hydroxyphenyl ring system makes largely hydrophobic interactions with Ile-267(7.32), Met-270(7.35), and His-264(6.66) in the upper region of the binding cavity and a polar interaction with a crystallographic water molecule. Of note are high crystallographic *B*-factors in the 4-hydroxyphenyl moiety (>100 Å^2) pointing to its high conformational flexibility even in the receptor-bound state. This is in line with previous structure-activity relationships studies, which established a variety of substituents in this position for high affinity triazolotriazine-like antagonists (16–17), as well as low amino acid sequence conservation of the 4-hydroxyphenyl ring contact residues between adenosine subtypes and vertebrate species (Fig. 3). Taken together with the results reported here that demonstrate the importance of the residues in the lower region of the binding cavity for the strength of ligand binding, these observations suggest that interactions in the upper region of the binding pocket are less important for ligand binding affinity, but rather contribute to A_{2A}AR ligand specificity.

Some of the above interactions have already been correctly identified through mutagenesis studies of the human A_{2A}AR prior to the determination of the crystal structure (2). In particular, Glu-169(5.30), His-250(6.52), Asn-253(6.55), and Ile-274(7.39), which are conserved among the vertebrate ARs (Fig. 3), have been directly implicated previously by both mutagenesis studies and modeling/structure-activity relationship studies (15, 18–20). However, the crystal structure also establishes a

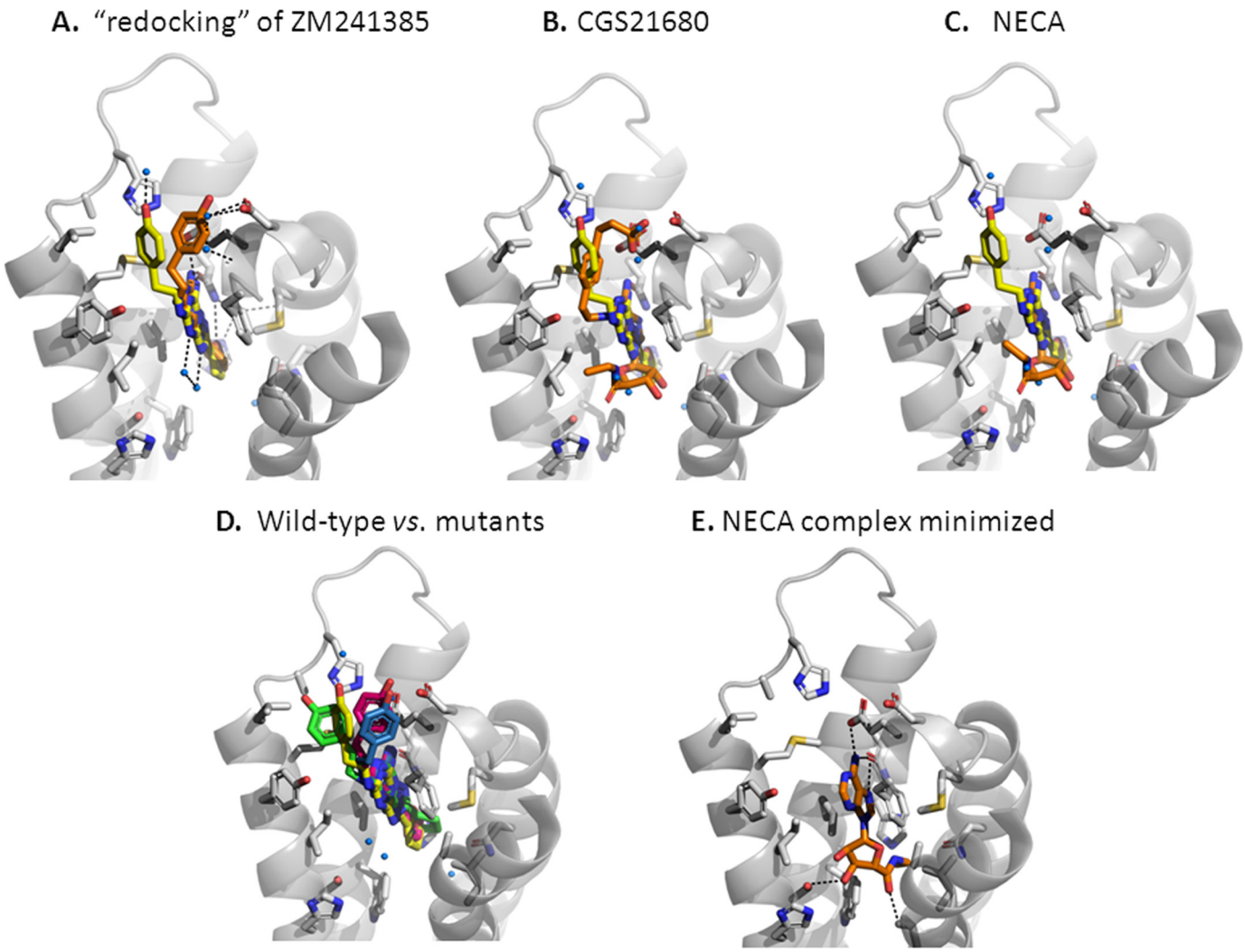

FIGURE 4. **Crystallographic structure-based molecular model of the human A_{2A}AR containing "docked" antagonist ZM241385, agonist NECA, and agonist CGS21680 bound in the antagonist-binding cavity.** Only parts of TM3, TM5, TM6, TM7, and a selected set of side chains in these TMs are shown. *A*, structural alignment of computationally re-docked ZM241385 (*orange*) in the experimental-binding cavity of co-crystallized ZM241385 (*yellow*). The polar interactions between ZM241385, crystallographic water molecules, and receptor are shown as *black dotted lines*. Docking was done using the FlexX program, including rigid side chains within 9 Å from the original ZM241385-binding cavity and with default protonation state (pH 7.0) as described under "Experimental Protocols." Note the different orientation of the 4-hydroxyphenyl group extension of ZM241385. *B* and *C*, superimposition of computationally docked agonists CGS21680 (*B*, *orange*) and NECA (*C*, *orange*) and co-crystallized ZM241385 (*yellow*) in the binding cavity. Only the automatic top solution produced by FlexX is shown. The other solutions alter the position and interactions of the ribose motif of NECA/CGS21680 and the C2-substituent of CGS21680. In all solutions the ribose motif is occupying different positions from the furan ring of ZM241385. *D*, influence of studied Ala mutations on the orientation of ZM241385 upon re-docking. Re-docked ZM241385 is shown in *purple* for the Phe-168(5.29) → Ala mutant, *green* for the Met-177(5.38) → Ala mutant, and *blue* for the Leu-249(6.51) → Ala mutant, ZM241385 from the co-crystal structure is shown in *yellow*. The orientation of the bicyclic core of ZM241385 is similar in all of the re-docking studies. *E*, energy minimization of the hypothetical NECA-receptor complex creates polar interactions (*black dotted lines*) between NECA (*orange*) and receptor residues Thr-88/Ser-277.

number of interactions unknown before in ZM241385 ligand recognition, involving eight uncharacterized residues. This prompted us to evaluate the functional importance of these residues in non-xanthine and xanthine ligand binding. In this report, residues Phe-168(5.29), Met-177(5.38), and Leu-249(6.51), which are located in the lower part of the ZM241385-binding cavity, and not previously reported on, were targeted for site-directed mutagenesis.

The importance of Phe-168(5.29) to ligand binding had not been fully recognized prior to the determination of the crystal structure of A_{2A}AR, although conservation of this amino acid between all known sequences of AR subtypes/species (Fig. 3*A*) and homology modeling studies provided some hints for its involvement in ligand binding (15). Our results demonstrate the essential role of the Phe-168(5.29) side chain in extracellular loop 2 in ligand binding. Interestingly, based on normalized occluded surface calculations in the crystal structure, Phe-168(5.29) has the highest contact area with ZM241385 and contributes an aromatic π-stacking interaction with the central triazolotriazine unit of ZM241385 (Fig. 2*B*). The calculated contribution of Phe-168(5.29) to binding is >6 kcal/mol, or ~25% of total binding energy for ZM241385 (Table 1). Furthermore, our radioligand binding and functional experiments using receptors with mutations at Phe-168(5.29) show the importance of aromatic stacking and hydrogen bonding to ligand binding. The Phe-168(5.29) → Trp mutation retained wild-type agonist and antagonist-binding properties and signaling function even though tryptophan has a much

TABLE 6
Predicted effect of mutations in residues Phe-168(5.29), Leu-249(6.51), and Met-177(5.38) on free energy antagonist and agonist binding

	Mutation	ZM241385 $\Delta\Delta G_{binding}$	CGS21680 $\Delta\Delta G_{binding}$	NECA $\Delta\Delta G_{binding}$
		kcal/mol	*kcal/mol*	*kcal/mol*
Phe-168(5.29)	Ala	5.9	5.4	4.7
	Val	4.5	5.8	5.0
	Tyr	0.3	0.5	0.1
	Trp	0.3	0.2	2.7
	Leu	5.5	7.3	10.
	Met	4.5	9.1	9.4
Leu-249(6.51)	Ala	3.3	2.9	3.6
	Val	1.2	0.36	1.4
	Tyr	14.	56.	7.4
	Phe	6.0	23.36	7.8
	Trp	74.0	37.3	7.1
	Met	−0.6	1.7	−0.4
Met-177(5.38)	Ala	1.4	1.4	1.0
	Val	−0.7025	0.7453	0.7
	Tyr	0.842	0.2536	1.9
	Phe	2.486	0.5106	1.9
	Trp	6.308	12.04	4.4
	Leu	4.047	−1.626	0.9

bulkier side chain. Our modeling studies (Fig. 4 and Table 6) show that tryptophan comfortably fits in the A_{2A}AR structure without major rearrangement of other residues. The mutation of Phe-168(5.29) to tyrosine, comparable in size and aromatic stacking properties to phenylalanine but with different hydrogen bonding capabilities, modulated agonist binding, antagonist binding, and functional properties resulting in a receptor with a moderately lower affinity for all ligands. In contrast, mutation of this phenylalanine to alanine resulted in a complete inability to measurably bind the radiolabeled antagonist [^{3}H]ZM241385, although intracellular cAMP accumulation assays reveal that this mutant could still bind the A_{2A}AR agonist CGS21680 and activate receptor-mediated G protein signaling, albeit with a 63-fold lower potency than the wild-type receptor. These results suggest that the aromatic stacking interactions between Phe-168(5.29) and the heterocyclic core of "classic" adenosine ligands are essential for both adenosine agonist and antagonist high affinity binding and agonist function.

The second largest normalized occluded surface interface between receptor residue and ZM241385 is with Leu-249(6.51), which is calculated to be 70% of the Phe-168(5.29) normalized occluded surface area (Fig. 2*B*). Leu-249(6.51) is located almost opposite to Phe-168(5.29) with respect to ZM241385 and makes hydrophobic interactions with the central triazolotriazine unit of the ligand. However, unlike Phe-168(5.29) the leucine residue in this position is not absolutely conserved (Fig. 3), with a valine residue occurring in the human A_{2B}AR. This is suggestive of a size restriction in this position. Although a role for this residue in ligand binding was suggested by Kim and co-workers, the specific nature of the interaction was not described (15). Here, the substitution to the small and less hydrophobic alanine residue abolished radioligand binding, suggesting strong structural requirements at this position in the triazolotriazine-binding cavity. However, in the cAMP accumulation assay a functional response for the agonist CGS21680 was retained for this mutant, although at 10-fold lower potency. The elimination of ligand binding and reduction of receptor activity upon mutation of Leu-249(6.51) to alanine suggests that this residue is vital for high affinity binding of the both the antagonist ZM241385 and the agonist CGS21680, although the agonist does retain some functional activity, suggesting that this residue is not as critical for agonist binding as for antagonist binding.

A third previously uncharacterized residue in the lower part of the ZM241385-binding cavity is Met-177(5.38), which is conserved throughout the AR family. Based on the crystal structure, Met-177(5.38) interacts with the furan ring of ZM241385 and is calculated to have 27% of the Phe-168(5.29) binding surface. As predicted by this more modest contact area, the alanine mutation only moderately reduced [^{3}H]ZM241385 binding affinity and had no significant effect on the affinity of the agonist NECA. Intriguingly, the Met-177(5.38) → Ala mutation had a significant effect on both the affinity and potency (6- and 7-fold respectively) of the A_{2A}AR-selective agonist CGS21680. As the model of agonist binding in Fig. 4 suggests, the ethylcarboxamide substituent at the C4′ position in the ribose ring of both CGS21680 and NECA makes a direct contact with the Met-177(5.38) side chain, explaining the modest sensitivity to mutation of this residue. Although NECA is also predicted to make this contact with Met-177(5.38), the lack of a bulky substituent in the adenine ring of NECA may allow more conformational flexibility in the receptor. This lack would also compensate for the lost contact in the Met-177(5.28) → Ala mutant, whereas the bulky substituent on the adenine ring of CGS21680 limits the conformations accessible to the receptor binding pocket.

Our results suggest that the binding mode of the triazolotriazine (antagonist) and adenine (agonist) cores is highly conserved, with Phe-168(5.29) making important interactions with both selective and non-selective agonists and antagonists. In contrast, the mutagenesis data along with the docking results suggest that the agonist ribose moiety is not in the same location as the furan ring of ZM241385, and that the Met-177(5.38)-ribose interaction is different from the Met-177(5.38)-furan ring interaction. It is tempting to speculate that the very hydrophilic ribose moiety, so important for receptor activation, would be located where the crystallographic water network in the lower part of the binding pocket resides, and our docking studies as well as previously published docking studies (15) support this localization. In our docking studies we find the ribose moiety in an orientation in which significant interactions are made with residues Thr-88(3.36), Ser-277(7.42), and His-278(7.43), close to the water network mentioned above. All three residues have previously been mutated and have been shown to be critically involved in agonist binding (20–22). Indeed mutation of Thr-88(3.36) or Ser-277(7.42) results in a substantial decrease in agonist but not antagonist binding and potency (22). However, it should be noted that we cannot predict conformation changes followed by agonist binding.

Furthermore, in one such study a "neoceptor" was generated by mutation of Thr-88(3.36) to aspartate, which responded to a positively charged aminosugar agonist derivative, again confirming the important interaction between this residue and agonist ligands (14, 15). However, without an agonist-occupied structure, it remains unclear to what extent structural rearrangements in the binding cavity occur upon binding of an ago-

nist and, consequently, what the exact atomic interactions would be.

The results of this study validate the key roles of Phe-168(5.29) and Leu-249(6.51) side-chain interactions with antagonists such as ZM241385 that were observed in the crystal structure, and demonstrate their equal importance for agonist binding. This suggests that the heterocyclic scaffold of both agonists and antagonists interact with the same core group of residues, and therefore this part of the ligand is in a very similar position for both agonists and antagonists. The modest selectivity of ZM241385 between A_{2A}AR and A_{2B}AR has risen from very small amino acid variations in the binding cavity; potentially in positions 6.51 (in lower part of cavity) and 7.32 (upper part). Clearer differences are seen between A_{2A}AR and A_3AR, where critical positions 5.30, 6.52, and 7.32 differ. Without a doubt, it would be beneficial to produce more antagonist co-structures, although an agonist-occupied structure would provide greater impact. In the absence of a crystal structure of the A_{2A}AR with an agonist bound, this study provides useful information to allow successful ligand docking studies at this receptor for both agonists and antagonists. This information, then, adds to the knowledge gained from the crystal structure and will aid in the design of more selective ligands for this important drug target.

Acknowledgments—We thank Jeffrey Velasquez, Mark Griffith, Tam Trinh, and Kirk Allin for technical help and Dr. Michael Hanson for initial help with normalized occluded surface data analysis. We acknowledge Angela Walker and Dr. A. Pia Abola for assistance with manuscript preparation and Raymond Benoit for laboratory management.

REFERENCES

1. Fredholm, B. B., Chen, J. F., Masino, S. A., and Vaugeois, J. M. (2005) *Annu. Rev. Pharmacol. Toxicol.* **45,** 385–412
2. Fredholm, B. B., Ijzerman, A. P., Jacobson, K. A., Klotz, K. N., and Linden, J. (2001) *Pharmacol. Rev.* **53,** 527–552
3. Jaakola, V. P., Griffith, M. T., Hanson, M. A., Cherezov, V., Chien, E. Y., Lane, J. R., Ijzerman, A. P., and Stevens, R. C. (2008) *Science* **322,** 1211–1217
4. Katritch, V., Jaakola, V. P., Lane, J. R., Lin, J., IJzerman, A. P., Yeager, M., Kufareva, I., Stevens, R. C., and Abagyan, R. (2010) *J. Med. Chem.* **53,** 1799–1809
5. Ballesteros, J. A., Weinstein, H., and Stuart, C. S. (1995) in *Receptor Molecular Biology* (Sealfon, S. C., ed) pp. 366–428, Academic Press, San Diego, CA
6. Hanson, M. A., and Stevens, R. C. (2009) *Structure* **17,** 8–14
7. Martinelli, A., and Tuccinardi, T. (2008) *Med. Res. Rev.* **28,** 247–277
8. Yuzlenko, O., and Kieæ-Kononowicz, K. (2009) *J. Comput. Chem.* **30,** 14–32
9. Michino, M., Abola, E., Brooks, C. L., 3rd, Dixon, J. S., Moult, J., and Stevens, R. C. (2009) *Nat. Rev. Drug Discov.* **8,** 455–463
10. Hanson, M. A., Brooun, A., Baker, K. A., Jaakola, V. P., Roth, C., Chien, E. Y., Alexandrov, A., Velasquez, J., Davis, L., Griffith, M., Moy, K., Ganser-Pornillos, B. K., Hua, Y., Kuhn, P., Ellis, S., Yeager, M., and Stevens, R. C. (2007) *Protein Expr. Purif.* **56,** 85–92
11. Abagyan, R., and Kufareva, I. (2009) *Methods Mol. Biol.* **575,** 249–279
12. Katritch, V., Reynolds, K. A., Cherezov, V., Hanson, M. A., Roth, C. B., Yeager, M., and Abagyan, R. (2009) *J. Mol. Recognit.* **22,** 307–318
13. Cheng, Y., and Prusoff, W. H. (1973) *Biochem. Pharmacol.* **22,** 3099–3108
14. Ivanov, A. A., Barak, D., and Jacobson, K. A. (2009) *J. Med. Chem.* **52,** 3284–3292
15. Kim, S. K., Gao, Z. G., Van Rompaey, P., Gross, A. S., Chen, A., Van Calenbergh, S., and Jacobson, K. A. (2003) *J. Med. Chem.* **46,** 4847–4859
16. de Zwart, M., Kourounakis, A., Kooijman, H., Spek, A. L., Link, R., von Frijtag Drabbe Künzel, J. K., and Ijzerman, A. P. (1999) *J. Med. Chem.* **42,** 1384–1392
17. Mantri, M., de Graaf, O., van Veldhoven, J., Göblyös, A., von Frijtag Drabbe Künzel, J. K., Mulder-Krieger, T., Link, R., de Vries, H., Beukers, M. W., Brussee, J., and Ijzerman, A. P. (2008) *J. Med. Chem.* **51,** 4449–4455
18. Jiang, Q., Lee, B. X., Glashofer, M., van Rhee, A. M., and Jacobson, K. A. (1997) *J. Med. Chem.* **40,** 2588–2595
19. Kim, J., Jiang, Q., Glashofer, M., Yehle, S., Wess, J., and Jacobson, K. A. (1996) *Mol. Pharmacol.* **49,** 683–691
20. Kim, J., Wess, J., van Rhee, A. M., Schöneberg, T., and Jacobson, K. A. (1995) *J. Biol. Chem.* **270,** 13987–13997
21. Gao, Z. G., Jiang, Q., Jacobson, K. A., and Ijzerman, A. P. (2000) *Biochem. Pharmacol.* **60,** 661–668
22. Jiang, Q., Van Rhee, A. M., Kim, J., Yehle, S., Wess, J., and Jacobson, K. A. (1996) *Mol. Pharmacol.* **50,** 512–521

Ligand Binding and Subtype Selectivity of the Human A_{2A} Adenosine Receptor: IDENTIFICATION AND CHARACTERIZATION OF ESSENTIAL AMINO ACID RESIDUES

Veli-Pekka Jaakola, J. Robert Lane, Judy Y. Lin, Vsevolod Katritch, Adriaan P. IJzerman and Raymond C. Stevens

J. Biol. Chem. 2010, 285:13032-13044.
doi: 10.1074/jbc.M109.096974 originally published online February 10, 2010
